ACS APPLIED MATERIALS & INTERFACES

Research Article

www.acsami.org

Electronically Type-Sorted Carbon Nanotube-Based Electrochemical Biosensors with Glucose Oxidase and Dehydrogenase

Hitoshi Muguruma,* Tatsuya Hoshino, and Kohei Nowaki

Department of Electronic Engineering, Shibaura Institute of Technology, 3-7-5 Toyosu, Koto-ku, Tokyo 135-8548, Japan

Supporting Information

ABSTRACT: An electrochemical enzyme biosensor with electronically type-sorted (metallic and semiconducting) single-walled carbon nanotubes (SWNTs) for use in aqueous media is presented. This research investigates how the electronic types of SWNTs influence the amperometric response of enzyme biosensors. To conduct a clear evaluation, a simple layer-by-layer process based on a plasma-polymerized nano thin film (PPF) was adopted because a PPF is an inactive matrix that can form a well-defined nanostructure composed of SWNTs and enzyme. For a biosensor with the glucose oxidase (GOx) enzyme in the presence of oxygen, the response of a metallic SWNT-GOx electrode was 2 times larger than that of a semiconducting SWNT-GOx electrode. In contrast, in the absence of oxygen, the response of the semiconducting SWNT-GOx electrode was retained, whereas that of the metallic SWNT-GOx electrode was significantly reduced. This indicates that direct electron transfer occurred with the semiconducting SWNT-GOx electrode, whereas the metallic SWNT-GOx electrode was dominated by a hydrogen peroxide pathway caused by an enzymatic reaction. For a biosensor with the glucose dehydrogenase (GDH; oxygen-independent catalysis) enzyme, the response of the semiconducting SWNT-GDH electrode was 4 times larger than that of the metallic SWNT-GDH electrode. Electrochemical impedance spectroscopy was used to show that the semiconducting SWNT network has less resistance for electron transfer than the metallic SWNT network. Therefore, it was concluded that semiconducting SWNTs are more suitable than metallic SWNTs for electrochemical enzyme biosensors in terms of direct electron transfer as a detection mechanism. This study makes a valuable contribution toward the development of electrochemical biosensors that employ sorted SWNTs and various enzymes.

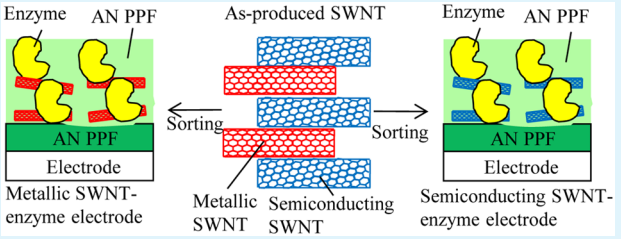

KEYWORDS: *electronic type-sorted carbon nanotubes, plasma-polymerized film, amperometric biosensor, glucose oxidase, glucose dehydrogenase*

INTRODUCTION

The advent of single-walled carbon nanotubes (SWNTs) has led to many new technical developments and applications due to their unique electronic properties, special geometry (high surface area-to-volume ratio), high mechanical strength, and chemical stability. SWNTs are conceptually thought to be the result of folding single graphene sheets into carbon cylinders. The directional variety of the folding (so-called chirality) causes electrically heterogeneous properties, that is, metallic SWNTs (mSWNTs) and semiconducting SWNTs (sSWNTs).[1,2] The as-produced SWNTs are typically a mixture of approximately one-third metallic and two-thirds semiconducting. The electronic density of states in sSWNTs exhibits a band gap near the Fermi level and near-infrared absorption. The conductance and valence bands in mSWNTs overlap each other, and mSWNTs exhibit high conductivity. Beyond electrical conductivity, mSWNTs and sSWNTs also differ in many other properties, such as chemical reactivity and the adsorption of molecules.[1]

A method of sorting SWNTs according to their electrical properties has been developed, and electronically homogeneous SWNTs (i.e., mSWNTs and sSWNTs) have been successfully harvested. One of the most useful procedures with regard to reproducibility and extension to mass production is a postproduction separation method known as density gradient ultracentrifugation (DGU), which was developed by Hersam and co-workers.[3,4] There have been reports on the applications of electronically homogeneous SWNTs.[1,2] Transparent conductive films with mSWNTs exhibited a more stable and lower sheet resistance than those with sSWNTs and unsorted (as-produced) SWNTs.[5−7] In contrast, a thin-film field effect transistor with sSWNTs had higher drive currents and a larger on/off current ratio than the mSWNT and unsorted SWNT counterparts.[3,4,8] The small on/off ratio of mSWNTs is considered to be due to the charge transport being dominated by metallic pathways. Only sSWNTs are applicable for phonic devices because of their energy band gap corresponding to the near-infrared region.[9−11] Thus, chemical sensors with sSWNTs as an active material (detection element) exhibit higher performance than those with unsorted SWNTs.[12,13] It has also been reported that devices with specific chirality (*n*,*m*)-enriched SWNTs demonstrate more advantages.[14−16]

Received: October 1, 2014
Accepted: December 18, 2014
Published: December 18, 2014

DOI: 10.1021/am506758u
ACS Appl. Mater. Interfaces 2015, 7, 584−592

Electrochemical (amperometric) biosensors with biospecific enzyme reactions have become an active research area because of their wide application, such as in medicine, environmental studies, agriculture, and fermentation.[17,18] There have been many reports of electrochemical enzyme-based biosensors that employ SWNTs.[19−23] The typical structure of an SWNT-based electrochemical biosensor involves a combination of biomacromolecules (e.g., enzymes) and SWNTs in the vicinity of the electrode (electron collector).[19−25] Biosensors function in an aqueous phase; therefore, the inherent insolubility and hydrophobicity of SWNTs has posed a significant challenge to their solution-phase manipulation. The approach to overcome this problem is the noncovalent chemical functionalization of SWNTs with functional polymers (e.g., polyethylenimine,[26,27] polythiophene,[28] and polyvinylpyridine[29]). Subsequent processes, such as immobilization of the redox sites and enzymes facilitate high performance. However, most electrochemical enzyme biosensors have employed electronically heterogeneous (unsorted) SWNTs, and less work has been conducted on an electrochemical enzyme-base biosensor with electronically type-sorted SWNTs. This article addresses how electronically type-sorted SWNTs affect the performance of electrochemical enzyme biosensors.

We have reported a biosensor based on a plasma-polymerized thin film (PPF) and/or plasma modification with SWNTs.[22,23] PPFs were prepared in a glow discharge under a monomer vapor phase, which resulted in the direct deposition of a thin film on a substrate. Direct plasma modification of SWNTs can change their hydrophobicity to hydrophilicity, while not significantly altering their electrical properties. Consequently, the working electrode of the biosensor exhibited excellent performance, due to excellent electrochemical contact between the reaction center of the enzyme and the SWNT layer.[22,23]

Investigation of the effectiveness of electrochemical biosensors with electronically type-sorted SWNTs is considered to be a challenging task. Our concern is that they may provide only elusive results, partly because those biosensors work in aqueous media unlike other electronic and photonic devices that work in atmosphere. Therefore, we adopted a simple layer-by-layer process based on PPFs, which is expected to be suitable for achieving a solution to this issue because a PPF as an inactive matrix provides a well-defined nanostructure that involves the SWNTs and enzymes. Two enzymes were selected as a benchmark, namely, glucose oxidase (GOx) and glucose dehydrogenase (GDH). These are the most common enzymes used as the biological component in electrochemical glucose biosensors to assist diabetes mellitus patients to monitor their daily sugar levels.

EXPERIMENTAL SECTION

Materials. Distilled water, potassium dihydrogen phosphate, disodium hydrogen phosphate, D-glucose, ethanol, hydrogen peroxide, ammonia, ascorbic acid, uric acid, acetaminophen, and acetonitrile were purchased from Kanto Chemical Co., Inc. (Tokyo, Japan). GOx obtained from *Aspergillus niger* (EC 1.1.3.4, type VII−S, 181 600 units g^{-1}, Sigma, St. Louis, MO) was used as an enzyme. NAD(P)-dependent GDH from *Bacillus sp.* (EC 1.1.1.47) was purchased from Wako (Osaka, Japan). NAD^+ (oxidized form) was purchased from Sigma (St. Louis, MO, USA). Electronically type-sorted SWNTs (IsoNanotube-M and IsoNanotube-M) were purchased from Nanointegris Inc. (Skokie, IL).[3] The surfactant is the mixture of sodium dodecyl sulfate and sodium cholate. The as-purchased solutions of type-sorted SWNTs were concentrated to achieve the desired concentration. The procedure for concentrating to achieve the desired concentration is as follows. A solution (100 mL) of type-sorted SWNTs (0.01 mg/mL) is attached to the evaporator. The solvent is evaporated at reduced pressure so as to be 1 mL in volume. The enrichment of concentration is available up to 1 mg/mL. When the concentration surpasses 1 mg/mL, aggregation and bundling of SWNT molecule occurs. Photographs of the electronically type-sorted SWNT solutions in vials are shown in Figure S1 (Supporting Information). Electronically type-sorted SWNTs were produced by arc-discharge, and their diameters and lengths were 1.2−1.7 nm and 0.3−4 μm, respectively. All reagents were used without further purification.

Fabrication Procedure. The electrochemical device as a working electrode was fabricated using a layer-by-layer process. The device was formed on a 0.15 mm thick glass substrate (ca. 50 × 50 mm^2). All metal layers were sputter-deposited and patterned using a masking process. The glass slides used to make the thin film electrodes were boiled in a hydrogen peroxide/ammonia/water solution (ca. 1:1:8 v/v) for 1 h and then rinsed with water and acetone. Au thin films were sputtered with a plasma generator (VEP-1000, Ulvac, Inc., Tokyo, Japan). A 40 nm thick chromium intermediate layer was used to promote adhesion of the gold layer. The dimensions of the opening for the working electrode were 5 × 5 mm^2.

The plasma generator was also used to deposit a 2 nm thick acetonitrile PPF layer (first PPF layer) onto the sputtered Au electrode at 150 W and under a pressure of 0.6 Pa. Aqueous solutions of the sorted SWNTs containing 1% surfactant were used. The SWNT solution (1 mg mL^{-1}, optimized) was dropped onto the PPF surface and dried in a vacuum oven. The thickness of the resulting sorted-SWNT film was ca. 100 nm. Subsequently, the SWNT-adsorbed surface was treated by acetonitrile plasma using the following parameters: power, 100 W; flow rate, 15 mL min^{-1}; pressure, 0.6 Pa; exposure time, 30 s (thickness < 1 nm). The role of this PPF is surface modification than layer formation (polymerization). The enzyme solution (5 μL) was then added by dropping an aliquot of GOx (1820 units g^{-1}) or GDH (2000 units g^{-1}) in phosphate buffer (20 mM, pH 7.4) onto the film. One hour later, the device was washed with water. Finally, the enzyme-adsorbed surface was overcoated with a 6 nm thick acetonitrile PPF layer (second layer). The deposition parameters were as follows: power; 150 W, pressure; 0.6 Pa, exposure time; 150 s. The devices were stored in a refrigerator at 4 °C until use.

Measurements. Atomic force microscopy (AFM) was conducted in tapping mode in the ambient atmosphere using a commercial AFM system (NanoScope IIIaAFM Dimension 3000 stage system, Nihon Veeco KK, Tokyo, Japan). The scanning tip was equipped with an alternating current (AC) mode supersharp chip (Nanosensors Inc., Neuchatel, Switzerland). A scanning rate of 0.6 Hz was employed. AFM system software was used to analyze the image data and calculate defined features, such as the root-mean-square roughness values (R_{rms}) and the maximum z-range values (R_{max}). Electrochemical measurements (cyclic voltammetry (CV) and fixed potential) were performed with an electrochemical analyzer (ALS Instruments, 701A West Lafayette, IN) using a three-electrode configuration. Reference (Ag/AgCl, RE-1C) and counter (platinum wire) electrodes were purchased from Bioanalytical Systems Inc. Electrochemical measurements were conducted in a 5 mL vessel at ambient temperature (20 °C) using a phosphate buffer (20 mM, pH 7.4) as the supporting electrolyte. For GDH, 0.5 mM NAD^+ was added. To prepare samples at designated concentrations, stock glucose solutions of 2.5, 25, or 250 mM were successively added. Electrochemical measurements were performed at least four times. Electrochemical impedance spectroscopy (EIS) was conducted in the frequency range of 100 mHz to 100 kHz at a direct current potential of 0.25 V and an AC perturbation of 5 mV. The electrolyte was pH 7.0, 20 mM phosphate buffer solution containing 10 mM $K_3[Fe(CN_6)]/K_4[Fe(CN)_6]$ (1:1, v/v).

RESULTS AND DISCUSSION

Optimization of Amperometric Biosensor with Type-Sorted SWNTs. The amperometric biosensor based on type-

DOI: 10.1021/am506758u
ACS Appl. Mater. Interfaces 2015, 7, 584−592

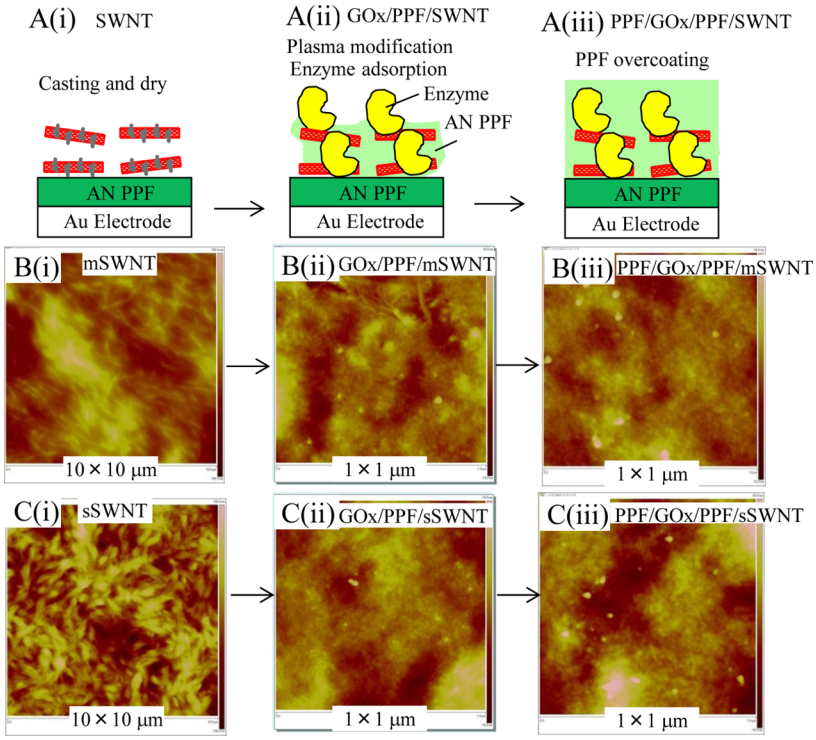

Figure 1. (A) Schematic representation of the fabrication process for an amperometric biosensor based on electronically type-sorted mSWNTs and sSWNTs, and PPF. (B, C) AFM images of the corresponding steps in (A). Horizontal scale: 10 × 10 μm (i), 1 × 1 μm (ii, iii). Vertical scale: 150 nm (i) and 20 nm (ii, iii).

sorted SWNTs and PPFs has a sandwich-like structure of PPF/GOx/SWNT/PPF/Au (SWNT-GOx electrode), and was fabricated using the layer-by-layer process shown in Figure 1A. The first PPF layer on the Au electrode acts as a scaffold for the formation of the SWNT layer. An SWNT layer cannot be obtained without the first PPF layer.[23] The method used for immobilization of the SWNTs on the electrode surface is to place a droplet of SWNT solution onto the electrode surface and allow it to evaporate. The utilization of surfactants for dispersion[29,30] can separate the bundles of SWNTs so that individual SWNTs can be obtained in solution. The surfactant is not only indispensable for dispersion but also versatile from a practical aspect to produce good surface properties.[31] Layers of type-sorted SWNT solutions containing surfactant had homogeneous surfaces compared with that prepared using a surfactant-free SWNT solution in Figure S2 (Supporting Information). The amount of SWNT loading was controlled according to the concentration of the SWNT solution. The loading of type-sorted SWNTs and GOx enzyme is a trade-off with regard to the contact area between them and the expression of SWNT functionality. Details for optimization of the resulting current are presented in Figure S3 (Supporting Information). Figure 1B,C shows AFM images of the surfaces of the type-sorted SWNT layers produced by drop-casting. SWNT networks were observed for both mSWNT and sSWNT surfaces. Although no distinct differences in alignment or uniformity were observed, the size of the sSWNT network was denser than that of the mSWNT network. This is related to the resulting sensor performance, as discussed in the following section.

Schmidtke and co-workers[30] reported that the surfactant sodium cholate is suitable for dispersing a relatively large surface area of SWNTs, but the hydrophobic naphthenic groups block the electronic signal. Bao and co-workers[14] reported that the postproduction separation method suffers from a low yield and difficulty in removal of the insulating sorting reagent. As a solution, we propose PPF modification of the surface of the sorted SWNT layer. An acetonitrile PPF modification period of 30 s, which corresponds to a thickness of ca. 1 nm, provides a highly nitrogen-rich surface (N/C ratio >0.2) investigated by X-ray photoelectron spectroscopy (XPS) measurements (Figure S4, Supporting Information). The effectiveness of the acetonitrile plasma modification was confirmed by CV in the presence and absence of glucose, as shown in Figure S5 (Supporting Information). The response of the SWNT-GOx electrode fabricated with acetonitrile plasma modification was several times larger than that without this step. Furthermore, higher sensitivity could be obtained than that with the SWNT electrode fabricated by the surfactant-free procedure (Figure S3); the surfactants play an important role for the better sensor performance. The reasons why acetonitrile plasma modification is effective are considered to be (i) the high-energy plasma changes the hydrophobic environment of the SWNTs and surfactant to a hydrophilic environment, and (ii) acetonitrile plasma modification results in a nitrogen-rich surface with positively charged (amino) groups,[32] which enables a dense loading of the negatively charged GOx (isoelectric point, pI = 4.2). In spite of importance of PPF modification, the role of SWNT still remains. This is supported by the fact that the response of GOx-PPF electrode (PPF/GOx/SWNT/PPF/Au) is 16-fold larger than that of GOx-PPF electrode containing no SWNT (PPF/GOx/PPF/Au).[32] Furthermore, the sensor response increases while the loading amount of SWNT increases in Figure S3. Therefore, the function of SWNT is not only so important acting as a scaffold

DOI: 10.1021/am506758u
ACS Appl. Mater. Interfaces 2015, 7, 584−592

to increasing the loading area but also as a functional material to increasing the current (sensitivity).

Figure 1B,C shows AFM images of the GOx enzyme molecules adsorbed onto the SWNT layer and onto the surface of a sorted SWNT layer modified by PPF as a densely packed two-dimensional array. This observation was similar to that which we previously reported for a very flat PPF surface where enzyme adsorption on the PPF surface follows a Langmuir isotherm.[33] Therefore, the plasma process is an effective strategy as an enzyme-friendly platform for SWNT-based electrochemical biosensors[22,23] and can replace time-consuming wet chemical procedures, such as that using polyethylenimine.[26,27] The final step was the overcoating of acetonitrile PPF onto the immobilized GOx and SWNTs. The GOx adsorbed on the surface was embedded and then immobilized within the second acetonitrile PPF layer. Figure 1B,C shows that the final sensing surface is very flat (R_{rms} < 3 nm). It was concluded that this fabrication process provides a well-defined sorted SWNT-enzyme complex for subsequent investigations.

Comparison of mSWNT and sSWNT for Amperometric Biosensor with the GOx Enzyme. The influence of the different electronic type SWNTs (mSWNTs or sSWNTs) on the electrochemical response of a biosensor was investigated for GOx, which is the most popular enzyme used in glucose sensing. Two mechanisms can be considered for the current response. One is the catalytic activity of the SWNTs[24,25] toward hydrogen peroxide generated by the enzymatic reaction; GOx specifically catalyzes the oxidation of glucose as follows:

$$\beta\text{-D-glucose} + O_2 \xrightarrow{\text{GOx}} \text{D-gluconic acid} + H_2O_2 \quad (1)$$

and the SWNT catalyzes the reaction of hydrogen peroxide as follows:

$$H_2O_2 \rightarrow 2H^+ + O_2 + 2e^- \quad (2)$$

The Au anode receives electrons, and the current increases. The other mechanism is direct electron transfer (DET) via the SWNTs, and a possible mechanism is

$$\beta\text{-D-glucose} + \text{GOx(FAD)} \rightarrow \delta\text{-gluconolactone} + \text{GOx(FADH}_2\text{)} \quad (3)$$

$$\text{GOx(FADH}_2\text{)} + 2M_{ox} \rightarrow \text{GOx(FAD)} + 2M_{red} + 2H^+ \quad (4)$$

$$2M_{red} \rightarrow 2M_{ox} + 2e^- \quad (5)$$

where flavin adenine dinucleotide (FAD) is located in the vicinity of the GOx reaction center, and M represents an electron-transfer mediator. This process is dominated under conditions of oxygen depletion. However, the DET process for GOx proteins is rarely observed on a bare electrode because the redox center of the enzyme is deeply embedded in a thick insulating protein shell, and the spacing between the prosthetic group (e.g., FAD) and the electrode surface generally exceeds the critical electron-tunneling distance.

CV is a useful tool for fundamental evaluation of the modified electrode. CV was performed to investigate how the electronic type SWNT layer would affect the electrochemical response of the enzyme electrode. The two mechanisms can be distinguished whether the oxygen is present or absent. The detection pathway is dominated by hydrogen peroxide route when the oxygen is present, whereas it is done by electron transport when the oxygen is absent. It can make sense to measure the current at the specific potential of CVs under oxygen presence or absence. Figure 2A shows CVs for the mSWNT-GOx and sSWNT-GOx electrodes in the presence of

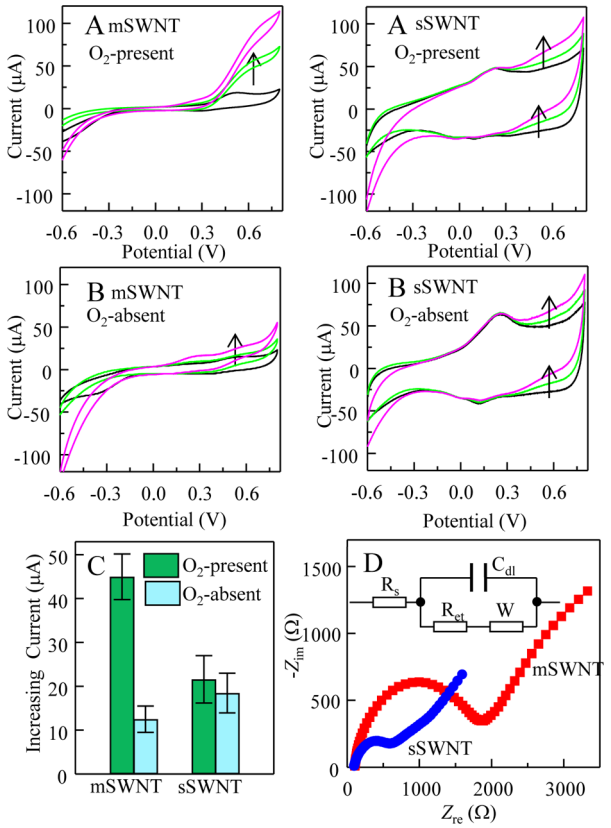

Figure 2. CV profiles for the GOx biosensor with (A) mSWNTs and (B) sSWNTs in the presence and absence of oxygen. Sweep rate: 50 mV s^{-1}. Glucose concentration: 0, 10, 48 mM. pH 7.4 phosphate buffer solution. (C) Comparison of sorted SWNT-GOx biosensor responses to 48 mM glucose in the presence and absence of oxygen at +0.6 V. (D) Nyquist plots and the equivalent electrical circuit (inset) from EIS measurements of biosensors with sorted SWNTs.

oxygen (air-saturated). At greater than +0.4 V, an increase in the current due to glucose addition was observed (Figure 2A). This is due to the oxidation of hydrogen peroxide generated by the enzymatic reaction, which corresponds to eqs 1 and 2. In this case, the SWNTs play a major role as a catalyst for the generation of hydrogen peroxide. The response of the mSWNT-GOx electrode was 2 times larger than that of the sSWNT-GOx electrode, which is probably due to its greater catalytic activity toward hydrogen peroxide generation, as shown in Figure S6 (Supporting Information). These results indicate a strong correlation between the mSWNT-GOx and sSWNT-GOx electrodes by their responses to glucose and hydrogen peroxide. Therefore, the detection mechanism in the presence of oxygen is dominated by the diffusion (transport) and oxidation of hydrogen peroxide generated by enzymatic reaction.

Figure 2B shows CVs for the mSWNT-GOx and sSWNT-GOx electrodes in the absence of oxygen (nitrogen-saturated). The CV characteristics for the mSWNT-GOx electrode are significantly different from those in the presence of oxygen (Figure 2A). The response to glucose was significantly decreased as shown in Figure 2C. In contrast, the CV profiles for the sSWNT-GOx electrode in both the presence and the absence of oxygen were similar, so that the response to glucose

DOI: 10.1021/am506758u
ACS Appl. Mater. Interfaces 2015, 7, 584−592

was almost unchanged. In the CV profile for the sSWNT-GOx electrode in the absence of oxygen, the anodic and cathodic peaks were at 0.249 V (= E_{pa}) and 0.128 V (= E_{pc}), respectively, and the peak-to-peak separation (ΔE_p) was 0.121 V. These values were exactly the same as that for the sSWNT-GOx electrode in the presence of oxygen. In contrast, those peaks were not observed for the mSWNT-GOx or the unsorted SWNT-GOx electrodes. Additionally, those also were not observed for sSWNT-GOx electrode by less sSWNT loading (0.01 and 0.2 mg/mL) shown in Figure S3 (Supporting Information). The reason for these results has yet to be clarified, and the details of electron-transfer mechanism will be the next step; however, we speculate that it may be attributed to a redox potential produced by the electronically homogeneous sSWNT "network". Then, this network with electronically homogeneous SWNT easily form the conduction "band", which paves the easy way for electron-transfer route. To test this hypothesis, the characteristics of the redox reaction process were investigated by varying the scan rate. Figure S7 (Supporting Information) shows an increase in the linearity with the scan rate from 10 to 300 mV s^{-1}, which indicates that the redox reaction is a surface-controlled electrochemical process and that the redox signals originate from GOx immobilized on the sSWNT layer. Using the Laviron equation,[34] the electron-transfer rate constant (k_s) of the sSWNT-GOx electrode was calculated to be 3.0 s^{-1}, which is slightly better than that of other SWNT-based electrodes for DET (0.3[35] and 1.7[36] s^{-1}). The electroactive protein density (Γ, mol cm^{-2}) of the GOx/sSWNT electrode could be estimated using the following equation:[37]

$$I_p = \frac{n^2F^2\nu A\Gamma}{4RT} \quad (6)$$

where I_p is the peak current, A is the electrode area, F is the Faraday constant, R is the gas constant, T is the temperature, n is the number of electrons being transferred, and ν is the scan rate. The surface coverage of electroactive GOx is calculated to be 1.7×10^{-9} mol cm^{-2}, which is slightly larger than that of the unsorted and functionalized SWNT/GOx electrode (7.1×10^{-10} mol cm^{-2}) reported by Yan et al.[26] The surface coverage of GOx on the flat PPF was estimated to be 1.6×10^{-12} mol cm^{-2}, in which GOx is a densely packed monolayer with the shape of a compact ellipsoid with approximate dimensions of 12.2×8.3 nm^2 (empirically determined using AFM).[33] This indicates that the procedure involving PPF leads to a substantially higher surface coverage of enzyme. On the basis of measurements with a varied scan rate, the overall sensing mechanism of the sSWNT-GOx electrode suggests the possibility of DET represented by eqs 3−5. In addition, the similarity of the CV profiles with glucose addition to those for the SWNT/GOx electrode with DET supports our hypothesis.[38]

Electrochemical impedance spectroscopy (EIS) is a highly effective method used to probe the surface features of an electrode. EIS was conducted to investigate the electron-transfer properties of the mSWNT-GOx and sSWNT-GOx electrodes. Figure 2D shows typical impedance spectra, in the form of Nyquist plots, for biosensors with these electrodes. The small semicircular domain at high frequencies corresponds to an electron-transfer limited process, and the straight line at low frequencies corresponds to a diffusion process. The Randles equivalent circuit (Figure 2D, inset) was selected to fit the impedance data, where R_s is the solution resistance, R_{et} is the electron transfer resistance, W is the Warburg impedance, and C_{dl} is the double-layer capacitance. All data are summarized in Table S1 (Supporting Information). Calculated from the diameter of the semicircular domain in the Nyquist plot, the sSWNT-GOx electrode exhibited an R_{et} value of 0.93 kΩ, which was much smaller than that of the mSWNT-GOx electrode (R_{et} = 3.6 kΩ). Because of XPS data (Figure S4), there is no possibility that the mSWNTs adsorb more surfactant than sSWNTs, and that is the reason for the reduced conductivity; amount of sodium due to the surfactant (ratio of Na 1s/C 1s) was similar between mSWNT and sSWNT layer. The EIS data are not consistent with the electrical properties of the bulk SWNTs but that of SWNT network. Therefore, the electron transport to the sensing electrode with the hopping process is more easily achieved in the sSWNT network than in the mSWNT network.

Furthermore, sSWNT networks could form only when loading of sSWNT was optimized (1 mg/mL). For example, sSWNT-GOx electrode by less amount of sSWNT loading (0.01 mg/mL) showed the larger R_{et} (= 41 kΩ). The response of the sSWNT-GOx electrode by small sSWNT loading decreased with the oxygen depletion, suggesting the detection pathway dominated by the hydrogen peroxide (Figure S8, Supporting Information). In contrast, complete mSWNT network could not be realized even though it was optimized. One mg/mL is the maximum concentration for homogeneous solution; the CV response increased while the concentration increased up to 1 mg/mL shown in Figure S2. When the concentration surpasses 1 mg/mL, aggregation and bundling of SWNT molecule occurs. This situation is similar to surfactant-free SWNT dispersing solution. When the sensor response of more than 1 mg/mL SWNT suspension was fabricated, the background current was too large; as a result, response to glucose decreased (Figure S3, Supporting Information). In this case, R_{ct} was also increased. Again, the sensing mechanism of the mSWNT-GOx having incomplete SWNT network is determined by hydrogen peroxide pathway.

Additionally, the larger C_{dl} for the sSWNT-GOx electrode than for mSWNT-GOx electrode suggests a correlation with the larger background current (hysteresis) due to a large double-layer capacitance in the CV profile for the sSWNT-GOx electrode than that for the mSWNT-GOx electrode. The EIS data also correspond to the CV data in terms of DET of the sSWNT-GOx electrode.

In summary, SWNTs in an enzyme electrode act as both conductor and catalyst. In the presence of oxygen, mSWNTs and sSWNTs mainly function as a catalyst, and the response (current) is attributed to the diffusion and oxidation of hydrogen peroxide. In the absence of oxygen, the enzymatic reaction proceeds through an oxygen-independent pathway. In this case, electrons must transfer through the SWNTs to the electron collector (Au anode). Electron transport through the sSWNT network proceeds smoothly, whereas the mSWNT network is an obstacle in comparison. Although the proposed mechanism is hypothetic, the result can probably be applied to oxidase enzyme. It is noteworthy that DET was realized by the combination of PPF and sSWNT through a facile procedure.

Comparison of mSWNT and sSWNT for Amperometric Biosensor with the GDH Enzyme. Although GOx is the most common enzyme used as the biological component in glucose biosensors, it has a drawback in that its enzymatic reaction is strongly dependent on the concentration of dissolved oxygen as an electron acceptor. In contrast, the

DOI: 10.1021/am506758u
ACS Appl. Mater. Interfaces 2015, 7, 584−592

enzymatic reaction of the GDH enzyme is independent of dissolved oxygen. β-nicotinamide adenine dinucleotide (NADH) is a cofactor for a large number (more than 300) of NADH-dependent dehydrogenase enzymes. The NADH cofactor is generally present outside the enzyme, unlike the FAD cofactor of GOx, which is deeply embedded in a thick insulating protein shell. Consequently, DET with the dehydrogenase enzyme electrode is expected to be more easily performed than with the oxidase enzyme counterpart. Here, we investigate how the SWNT electronic type affects the amperometric characteristics of a biosensor with NADH-dependent GDH.

The sensing mechanism involves the peak at ca. +0.6 V due to the oxidation of NADH caused by enzymatic reaction. The sensor response is due to the following enzymatic reaction:

$$\beta\text{-D-glucose} + \mathrm{NAD^+} \xrightarrow{\mathrm{GDH}} \delta\text{-gluconolactone} + \mathrm{NADH} \quad (7)$$

The substrate (glucose) and coenzyme (NAD^+) were simultaneously positioned in the vicinity of the active site of the enzyme (GDH). NAD^+ is a major electron acceptor in the oxidation of glucose, and the nicotinamide ring of NAD^+ accepts a hydrogen ion and two electrons, equivalent to a hydride ion. The reduced form of this carrier generated by this reaction is NADH, which can be electrochemically oxidized at a polarized potential of ca. 0.6 V versus Ag/AgCl; that is, electron transfer occurs at the anode via SWNTs as in the following equation:

$$\mathrm{NADH} \rightarrow \mathrm{NAD^+} + \mathrm{H^+} + 2\mathrm{e^-} \quad (8)$$

The fabrication procedure is similar to that with GOx, where instead of GOx, a GDH solution was drop-cast onto the PPF-modified SWNT layer. Details for the optimization process are shown in Figure S9 (Supporting Information). It was confirmed that the response of the sorted SWNT-GDH electrodes was better than that of the unsorted SWNT-GDH electrodes. Figure 3A,B shows CV profiles for the mSWNT-GDH and sSWNT-GDH electrodes. Both electrodes showed an increase in current with glucose addition. The increase in current at ca. +0.6 V can be assigned to eqs 6 and 7.[39] This peak for the sSWNT-GDH electrode is more distinct than that for the mSWNT-GDH electrode. The current of the sSWNT-GDH electrode is 4 times larger than that of the mSWNT-GDH counterpart (Figure 3A–C). The EIS spectra in Figure 3D shows that the electron-transfer resistance of the enzyme electrode with mSWNT (R_{et} = 1.5 kΩ) is larger than that with sSWNT (R_{et} = 1.1 kΩ). Therefore, the EIS data have a strong correlation with the sensing response in terms of DET. In summary, sSWNT is more suitable than mSWNT for the GDH-based biosensor.

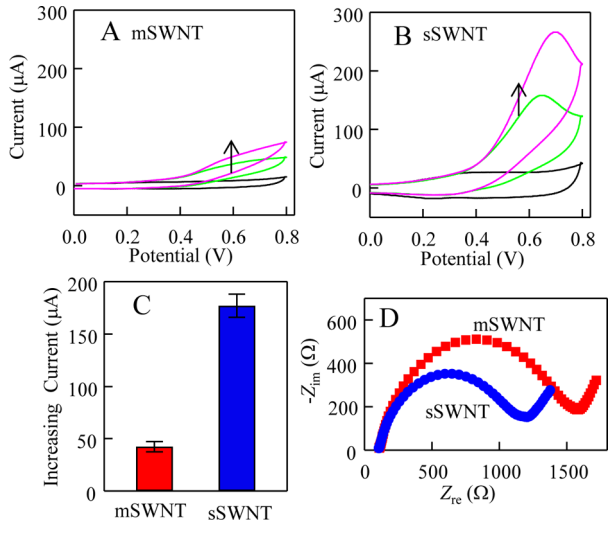

Figure 3. CV profiles for the GDH biosensor with (A) mSWNTs and (B) sSWNTs. (A). Sweep rate: 50 mV s^{-1}. Glucose concentration: 0, 10, 48 mM. pH 7.4 phosphate buffer solution. (C) Comparison of sorted SWNT-GDH biosensor responses to 48 mM glucose. (D) Nyquist plot of the GDH-biosensors with sorted SWNTs from EIS measurements.

Sensor Performance. The previous sections presented the optimization of the sensor fabrication process based on mSWNTs and sSWNTs. The sensitivity of the mSWNT-GOx electrode was better than that of the sSWNT-GOx electrode in the presence of oxygen. The sensitivity of the sSWNT-GDH electrode was better than that of the mSWNT-GDH counterpart. Here, the sensor performance of the optimized device is demonstrated. Amperometric measurements (time vs current) are widely used to evaluate and analyze the performance of glucose biosensors toward an increase in glucose concentration. Figure 4A shows the steady-state amperometric response of the fabricated mSWNT-GOx and sSWNT-GDH biosensors at +0.6 V versus Ag/AgCl. From the CV profiles in Figures 2 and 3, the potential at +0.6 V is available for time-based measurement with a fixed potential. A sequential increase in the glucose concentration at regular intervals is observed, of which the range of glucose concentrations can cover the physiological range. The small background current (0.4–0.8 μA) compared to the glucose response (3.6 and 15 μA at 1.4 mM glucose for the mSWNT-GOx and sSWNT-GDH electrodes, respectively) is a significant characteristic in the present results. This means that there is no need to calibrate the baseline for the glucose measurement. The detection limits (signal-to-noise (S/N) ratio = 3) of the mSWNT-GOx and sSWNT-GDH electrodes were 20 and 7.1 μM, respectively, when the S/N ratio was 3. The response time (95% to maximum response) was less than 7 s. The effect of interfering compounds (ascorbic acid, uric acid, and acetaminophen, Figure 4A) is negligible in the sensing characteristics (Figure 4A, inset) for use in physiological samples.

Figure 4B shows the current versus glucose concentration based on the data from Figure 4A. The sensitivities determined from the slopes for the sSWNT-GDH and mSWNT-GOx electrodes were 45 μA mM^{-1} cm^{-2} (r = 0.991 in the linear range of 0.25–2.5 mM) and 10 μA mM^{-1} cm^{-2} (r = 0.987 in the linear range of 0.25–1.4 mM), respectively. As mentioned in Supporting Information, Figure S4, kinetics for sensing indicates a surface-controlled process. Then, the reaction at the sensing surface is systematically discussed. We consider the following reaction sequence.

$$\mathrm{S_{bulk}} \xrightarrow{k_D} \mathrm{S_{surface}} + \mathrm{E_O} \xrightarrow{K_M} \mathrm{E_OS} \xrightarrow{k_C} \mathrm{E_R} + \mathrm{P} \quad (9)$$

where k_D denotes the rate constant for mass transport from solution (bulk) to the sensing surface, K_M denotes Michaelis constant, kc denotes catalytic rate constant. S denotes substrate (glucose), E_O denotes oxidized enzyme, E_OS denotes enzyme–substrate complex, E_R denotes reduced enzyme, and P denotes product from S. The substrate is free to diffuse through the film with a diffusion coefficient D, which is generally propositional

DOI: 10.1021/am506758u
ACS Appl. Mater. Interfaces 2015, 7, 584–592

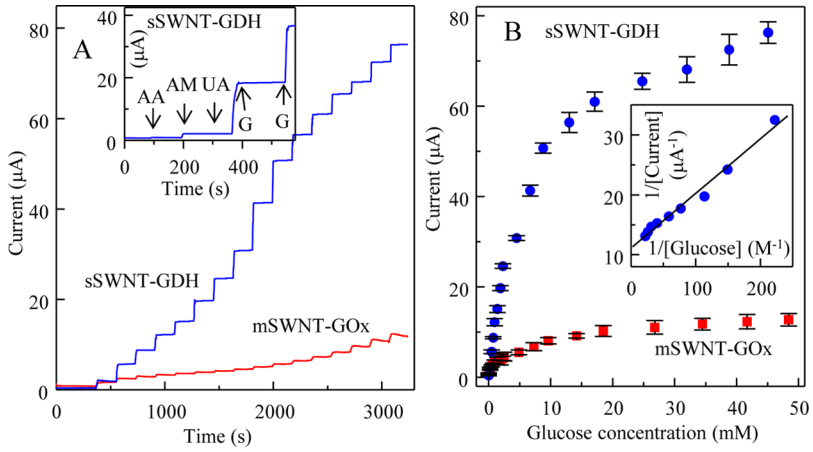

Figure 4. (A) Time-current response for sequential glucose (G) addition at concentrations of 0, 0.25, 0.49, 0.73, 0.96, 1.4, 1.9, 2.3, 4.5, 6.7, 8.8, 13, 17, 25, 32, 39, and 45 mM. (inset) The effect of an interferent species (0.1 mM ascorbic acid; AA, 0.1 mM acetaminophen; AM, and 0.1 mM uric acid; UA) on the response of sSWNT-GDH electrode. The concentrations of glucose (G) were sequentially 2.5 and 4.9 mM. The optimized electrode structure for the mSWNT-GOx and sSWNT-GDH electrodes is shown in Figure 1. The polarization potential was +0.6 V vs Ag/AgCl with an electrolyte of pH 7.4 20 mM phosphate buffer solution. (B) Calibration plot for glucose response using the data in A. The sensitivities of the mSWNT-GOx and sSWNT-GDH electrodes were 10 μA mM^{-1} cm^{-2} (r = 0.987 in the linear range of 0.25−1.4 mM) and 45 μA mM^{-1} cm^{-2} (r = 0.991 in the linear range of 0.25−2.5 mM), respectively. Each point represents the average, and the vertical bars designate the standard deviation (n = 4). (inset) Lineweaver−Burk plot for the mSWNT-GOx (I_{max} = 58 μA cm^{-2}, K_M^{app} = 8.2 mM) and sSWNT-GDH (I_{max} = 360 μA cm^{-2}, K_M^{app} = 8.1 mM) electrodes.

k_D. The diffusion of analyte molecules from bulk to sensing surface via enzyme/SWNT/PPF layer can be represented as a simple first-order diffusion equation based upon the Fick's First Law of Diffusion. The flux can be generated by application of a potential step and thus be measured by chronocoulometry. The relevant expression is as follows:[40]

$$J = D\frac{C_{bulk} - C_{surface}}{d} \quad (10)$$

where J is a flux of an analyte, $C_{surface}$ is its local concentration close to the electrode determined electrochemically, C_{bulk} is its bulk concentration, D is its diffusion constant, and d is the thickness of the diffucion layer. We have already estimated that the D of substrate in the system involving nanothin PPF by chlonocoulometry was 10^{-5}−10^{-6} cm^2/s.[41] Several nanometer-sized layer-by-layer structures of enzyme/SWNT/PPF electrode are very open, and so we can neglect concentration polarization of both substrate and SWNT within the enzyme layer.[42] Therefore, it can be assumed that the local concentration of the analyte on the electrode is zero ($C_{surface}$ = 0). The measured flux will be proportional to the substrate concentration as is usual in analytical chemistry. In fact, our sensor and the other with SWNT show the linear relationship in the range of lower concentration.

In contrast, saturation from linearity is observed at higher (>20 mM) glucose concentrations, which represents a typical characteristic of the Michaelis−Menten model. Since flux J is proportional the concentration of substrate, k_D surpasses k_S. This is a reaction-controlled step and can be applied to the Michaelis−Menten analysis. The inset of Figure 4B shows a Lineweaver−Burk plot (double reciprocal plot), from which the apparent Michaelis−Menten activity (K_M^{app}), as an indication of the enzyme−substrate kinetics for the biosensor, can be calculated as follows:

$$\frac{1}{I} = \frac{K_M^{app}}{I_{max}}\frac{1}{C} + \frac{1}{I_{max}} \quad (11)$$

where I is the steady-state current, I_{max} is the maximum current under stationary substrate conditions, K_M^{app} denotes the apparent Michaelis constant, and C is the glucose concentration. The I_{max} and K_M^{app} values were obtained from extrapolation of the plot shown in the inset of Figure 4B. K_M^{app} for immobilized GOx and GDH were thus estimated to be 8.2 and 8.1 mM, respectively, which are similar to those for other SWNT-based biosensors.[43−45] For GOx sensor, the 8.2 mM of K_M^{app} is smaller than that of free GOx (33 mM[43]). This is attributed to the affinity toward substrate of immobilized enzyme being increased relative to that of free enzyme.[43−45] For GDH sensor, the 8.1 mM of K_M^{app} is similar to that of free GDH (4.2−13 mM[46,47]), indicating that the affinity is not changed. The large I_{max} (58 and 360 μA cm^{-2} for the GOx and GDH electrodes, respectively) represents highly effective electronic contact. From the known surface coverage of the GOx/SWNT and GDH/SWNT units,[48] the turnover rates for electron transfer to the electrode were estimate to be approximately 750 and 1300 s^{-1}, respectively. These are close to the turnover rates of native GOx (700 s^{-1})[49] and GDH (430 s^{-1}).[47]

Most of the SWNT/enzyme-based glucose biosensors show too high sensitivity and are saturated at the cutoff value (~4 mM) in physiological level.[50,51] I think that this electrode is useful for monitoring hypoglycemia in emergency medical care or control in fermentation (under oxygen depletion). Additionally, this sensor also has the linear range at higher glucose concentration range. For example, the sensitivity was 1.3 μA mM^{-1} cm^{-2} (r = 0.981, the linear range of 4.9−20 mM). This can cover the sugar level for diabetes. Moreover, the expansion for dynamic range is possible with, for example, diffusion control layer. Therefore, the sensor having the high sensitivity is versatile.

The present sensors exhibited, at least, better performance than sensors with unsorted SWNTs, as shown in Table S2 (Supporting Information). Thus, the utilization of sorted SWNTs not only increases the sensitivity of the biosensor, but also reduces the working potential. Finally, it was confirmed

DOI: 10.1021/am506758u
ACS Appl. Mater. Interfaces 2015, 7, 584−592

that the electrochemical response of the devices that retained a current response due to continuous polarization at +0.6 V in the presence of 4.9 mM glucose was greater than 90% of the initial current after 24 h, as shown in Figure S10 (Supporting Information).

CONCLUSION

The effectiveness of electronically type-sorted SWNT electrochemical biosensors was demonstrated for the first time. The aim of this research was to determine whether mSWNTs or sSWNTs are suitable for specific amperometric biosensors. For biosensors with enzyme GOx in the presence of oxygen, the response of the mSWNT-GOx electrode was 2 times larger than that of the sSWNT-GOx electrode. In contrast, without oxygen, the response of the sSWNT-GOx electrode was retained, whereas that of the mSWNT-GOx electrode was significantly diminished. This indicates that DET proceeded with the sSWNT-GOx electrode, whereas the mSWNT-GOx electrode was dominated by the hydrogen peroxide route. For biosensors with the GDH enzyme, the response with the sSWNT-GDH electrode was 4 times larger than that with the mSWNT-GDH electrode. EIS measurements showed that the sSWNT network is less resistant to electron transfer than the mSWNT network. It was concluded that sSWNTs are more suitable than mSWNTs for an electrochemical enzyme biosensor with regard to DET for the detection mechanism. This is the first report that examines how different electronic types of SWNTs affect the electrochemical response of enzyme biosensors. The method presented here will be a significant contribution toward the development of electrochemical biosensors with electronically type-sorted SWNTs because research involving SWNTs is one of the most active fields. It can be easily extended to other biosensor devices that use other enzymes and proteins. Future work should involve control of other SWNT properties such as alignment, diameter, length, and specific chilarity as well as the combination with redox materials to achieve improved performance.

ASSOCIATED CONTENT

Supporting Information

Optimization for fabrication, XPS surface analysis, investigation of the response to hydrogen peroxide, photographs of SWNT solutions, and all EIS data. This material is available free of charge via the Internet at http://pubs.acs.org.

AUTHOR INFORMATION

Corresponding Author

*E-mail: muguruma@shibaura-it.ac.jp. Fax: +81-3-5859-8201.

Notes

The authors declare no competing financial interest.

REFERENCES

(1) Lu, F.; Meziani, M. J.; Cao, L.; Sun, Y.-P. Separated Metallic and Semiconducting Single-Walled Carbon Nanotubes: Opportunities in Transparent Electrodes and Beyond. *Langmuir* **2010**, *27*, 4339−4350.

(2) Schnorr, J. M.; Swager, M. Emerging Applications of Carbon Nanotubes. *Chem. Mater.* **2011**, *23*, 646−657.

(3) Arnold, M. S.; Green, A. A.; Hulvat, J. F.; Stupp, S. I.; Hersam, M. C. Sorting Carbon Nanotubes by Elelctronic Structure Using density Differentiation. *Nat. Nanotechnol.* **2006**, *1*, 60−65.

(4) Antaris, A. L.; Seo, J. T.; Green, A. A.; Hersam, M. C. Sorting Single-Walled Carbon Nanotubes by Electronic Type Using Nonionic, Biocompatible Block Copolymers. *ACS Nano* **2010**, *4*, 4725−4732.

(5) Miyata, Y.; Yanagi, K.; Maniwa, Y.; Katsura, H. Highly Stabilized Conductivity of Metallic Single Wall Carbon Nanotube Thin Films. *J. Phys. Chem. C* **2008**, *112*, 3591−3596.

(6) Rahy, A.; Bajaj, P.; Musselman, I. H.; Hong, S. H.; Sun, Y.-P.; Yang, D. J. Coating of Carbon Nanotubes on Flexible Substrate and Its Adhesion Study. *Appl. Surf. Sci.* **2009**, *255*, 7084−7089.

(7) Green, A. A.; Hersam, M. C. Colored Semitransparent Conductive Coatings Consisting of Monodisperse Metallic Single-Walled Carbon Nanotubes. *Nano Lett.* **2008**, *8*, 1417−1422.

(8) Engel, M.; Small, J. P.; Steiner, M.; Freitag, M.; Green, A. A.; Hersam, M. C.; Avouris, P. Thin Film Nanotube Transistors Based on Self-Assembled, Aligned, Semiconducting Carbon Nanotube Arrays. *ACS Nano* **2008**, *2*, 2445−2452.

(9) Bindl, D. J.; Wu, M.-Y.; Prehn, F. C.; Arnold, M. S. Efficiently Harvesting Excitons from Electronic Type-Controlled Semiconducting Carbon Nanotube Films. *Nano Lett.* **2011**, *11*, 455−460.

(10) Bindl, D. J.; Ferguson, A. J.; Wu, M.-Y.; Kopidakis, N.; Blackburn, J. L.; Arnold, M. S. Free Carrier Generation and Recombination in Polymer-Wrapped Semiconducting Carbon Nanotube Films and Heterojunctions. *J. Phys. Chem. Lett.* **2013**, *4*, 3550−3559.

(11) Lu, R.; Christianson, C.; Kirkeminde, A.; Ren, S.; Wu, J. Extraordinary Photocurrent Harvesting at Type-II Heterojunction Interfaces: Toward High Detectivity Carbon Nanotube Infrared Detectors. *Nano Lett.* **2012**, *12*, 6244−6249.

(12) Roberts, M. E.; LeMieux, M. C.; Bao, Z. Sorted and Aligned Single-Walled Carbon Nanotube Networks for Transistor-Based Aqueous Chemical Sensors. *ACS Nano* **2009**, *3*, 3287−3293.

(13) Ganzhorn, M.; Vijayaraghavan, A.; Dehm, S.; Hennrich, F.; Green, A. A.; Fichtner, M.; Voigt, A.; Rapp, M.; von Löhneysen, H.; Hersam, M. C.; Kappes, M. M.; Krupke, R. Hydrogen Sensing with Diameter- and Chirality-Sorted Carbon Nanotubes. *ACS Nano* **2011**, *5*, 1670−1676.

(14) Wang, H.; Koleilat, G.; Liu, P.; Jiménez-Osés, G.; lai, Y.-C.; Vosgueritchian; Fang, Y.; Park, S.; Houk, K. N.; Bao, Z. High-Yield Sorting of Small-Diameter Carbon Nanotubes for Solar Cells and Transistor. *ACS Nano* **2014**, *8*, 2609−2617.

(15) Park, J.; Deria, P.; Olivier, J.-H.; Therien, M. J. Fluence-Dependent Singlet Exciton Dynamics in Length-Sorted Chirality-Enriched Single-Walled Carbon Nanotubes. *Nano Lett.* **2014**, *14*, 504−511.

(16) Mehlenbacher, R. D.; Wu, M.-Y.; Grechko, M.; Laaser, J. E.; Arnold, M. S.; Zanni, M. T. Photoexcitation Dynamics of Coupled Semiconducting Carbon Nanotube Thin Films. *Nano Lett.* **2013**, *13*, 1495−1501.

(17) Sarma, A. K.; Vatsyayan, P.; Goswami, P.; Minteer, S. D. Recent Advances in Material Science for Developing Enzyme Electrodes. *Biosens. Bioelectron.* **2009**, *24*, 2313−2322.

(18) Kimmel, D. W.; LeBlanc, G.; Meschievitz, M. E.; Cliffel, D. E. Electrochemical Sensors and Biosensors. *Anal. Chem.* **2012**, *84*, 685−707.

(19) Wang, J.; Lin, Y. Functionalized Carbon Nanotubes and Nanofibers for Biosensing Applications. *Trends Anal. Chem.* **2008**, *27*, 619−626.

(20) Yan, X. B.; Chen, X. J.; Tay, B. K.; Khor, K. A. Transparent and Flexible Glucose Biosensor via Layer-By-Layer Assembly of multi-Wall Carbon Nanotubes and Glucose Oxidase. *Electrochem. Commun.* **2007**, *9*, 1269−1275.

(21) Claussen, J. C.; Franklin, A. D.; Haque, A.; Porterfield, D. M.; Fisher, T. S. Electrochemical Biosensor of Nanocube-Augmented Carbon Nanotube Networks. *ACS Nano* **2009**, *3*, 37−44.

(22) Muguruma, H.; Hoshino, T.; Matsui, Y. Enzyme Biosensor Based on Plasma-Polyemrized Film-Covered Carbon Nanotube Layer Grown Directly on A Flat Substrate. *ACS Appl. Mater. Interfaces* **2011**, *3*, 2445−2450.

(23) Muguruma, H.; Shibayama, Y.; Matsui, Y. Amperometric Biosensor Based on A Composite of Single-Walled Carbon Nanotubes, Plasma-Polymerized Thin Film, and An Enzyme. *Biosens. Bioelectron.* **2008**, *23*, 827−832.

DOI: 10.1021/am506758u
ACS Appl. Mater. Interfaces 2015, 7, 584−592

(24) Wang, J.; Musameh, M. Carbon Nanotube/Teflon Composite Electrochemical Sensors and Biosensors. *Anal. Chem.* **2003**, *75*, 2075−2079.
(25) Merkoçi, A.; Pumera, M.; Llopis, X.; Pérez, B.; Valle, M.; Alegret, S. New Materials for Electrochemical Sensing VI: Carbon Nanotubes. *Trend. Anal. Chem.* **2005**, *24*, 826−838.
(26) Yan, Y.-M.; Baravik, I.; Yehezkeli, O.; Willner, I. Integrated Electrically Contacted Glucose Oxidase/Carbon Nanotube Electrodes for the Bioelectrocatalyzed Detection of Glucose. *J. Phys. Chem. C* **2008**, *112*, 17883−17888.
(27) Tran, T. O.; Lammert, E. G.; Chen, J.; Merchant, S. A.; Brunski, D. B.; Keay, J. C.; Johnson, M. B.; Glatzhofer, D. T.; Schmidtke, D. W. Incorporation of Single-Walled Carbon Nanotubes into Ferrocene-Modified Linear Polyethylenimine Redox Polymer Films. *Langmuir* **2011**, *27*, 6201−6210.
(28) Pang, X.; Imin, P.; Zhitomirsky, I.; Adronov, A. Amperometric Detection of Glucose Using A Conjugated Polyelectrolyte Complex with Single-Walled Carbon Nanotubes. *Macromolecules* **2010**, *43*, 10376−10381.
(29) Tsai, T.-W.; Heckert, G.; Neves, L. F.; Tan, Y.; Kao, D.-Y.; Harrison, R. G.; Resasco, D. E.; Schmidtke, D. W. Adsorption of Glucose Oxidase onto Single-Walled Carbon Nanotubes and Its Application in Layer-By-Layer Biosensors. *Anal. Chem.* **2009**, *81*, 7917−7925.
(30) Chen, J.; Tran, T. O.; Ray, M. T.; Brunski, D. B.; Keay, J. C.; Hickey, D.; Johnson, M. B.; Glatzhofer, D. T.; Schmidtke, D. W. Effect of Surfactant Type and Redox Polymer Type on Single-WalledCarbon Nanotube Modified Electrodes. *Langmuir* **2013**, *29*, 10586−10595.
(31) Rouhi, N.; Jain, D.; Burke, P. J. High-Performance Semiconducting Nanotube Inks: Progress and Prospects. *ACS Nano* **2011**, *5*, 8471−8487.
(32) Muguruma, H.; Hiratsuka, A.; Karube, I. Thin Film Glucose Biosensor Based on Plasma-Polymerized Film: Simple Design for Mass Production. *Anal. Chem.* **2000**, *72*, 2671−2675.
(33) Muguruma, H.; Kase, Y.; Murata, N.; Matsumura, K. Adsorption of Glucose Oxidase onto Plasma-Polymerized Film Characterized by Atomic Force Microscopy, Quartz Crystal Microbalance, and Electrochemical Measurement. *J. Phys. Chem. B* **2006**, *110*, 26033−26039.
(34) Laviron, E. General Expression of the Linear Potential Sweep Voltammogram in the Case of Diffusionless Electrochemical Systems. *J. Electroanal. Chem.* **1979**, *101*, 19−28.
(35) Liu, J.; Chou, A.; Rahmat, W.; Paddon-Row, M. N.; Gooding, J. J. Achieving Direct Electrical Connection to Glucose Oxidas using Aligned Single Walled Carbon Nanotube Arrays. *Electroanalysis* **2005**, *17*, 38−46.
(36) Guiseppi-Elie, A.; Lei, C.; Baughman, R. H. Direct Electron Transfer of Glucose Oxidase on Carbon Nanotubes. *Nanotechnology* **2002**, *13*, 559−564.
(37) Laviron, E. The Use of Linear Potential Sweep Voltammetry and of A.C. Voltammetry for The Study of The Surface Electrochemical Reaction of Strongly Adsorbed Systems And of Redox Modified Electrodes. *J. Electroanal. Chem.* **1979**, *100*, 263−270.
(38) Guo, C. X.; Li, C. M. Direct Electron Transfer of Glucose Oxidase and Biosensing of Glucose on Hollow Sphere-Nanostructured Conducting Polymer/Metal Oxide Composite. *Phys. Chem. Chem. Phys.* **2010**, *12*, 12153−12159.
(39) Muguruma, H.; Yoshida, S.; Urata, M.; Fujisawa, K.; Matsui, Y. An Amperometric Biosensor for Glucose Based on A Composite Electrode of Glucose Dehydrogenase, Carbon Nanotubes, and Plasma-Polymerized Thin Films. *Electrochemistry* **2008**, *76*, 545−548.
(40) Stein, W. D. *Transport and Diffusion across Cell Membrane,* 1st ed; Academic Press Inc.: Orlando, FL, 1986.
(41) Muguruma, H.; Itazu, N.; Miura, S. Characterization of Diffusion-Controlled Mass Transport through Nanoporous and Nanothin Films Plasma-Polymerized on a Sputtered Platinum Electrode. *J. Phys. Chem. B* **2005**, *109*, 18839−18845.
(42) Lyons, M. G. L. Transport and Kinetics at Carbon Nanotube − Redox Enzyme Composite modified Electrode Biosensors. *Int. J. Electrochem. Sci.* **2009**, *4*, 77−103.
(43) Swoboda, B. E. P.; Massey, V. Oxidase from Aspergillus niger Purification and Properties of the Glucose. *J. Biol. Chem.* **1965**, *240*, 2209−2215.
(44) Hoshino, T.; Sekiguchi, S.; Muguruma, H. Amperometric Biosensor Based on Multilayer Containing Carbon Nanotube, Plasma-polymerized Film, Electron Transfer Mediator Phenothiazine, and Glucose Dehydrogenase. *Bioelectrochemistry* **2012**, *84*, 1−5.
(45) Du, P.; Wu, P.; Cai, C. A Glucose Biosensor Based on Electrocatalytic Oxidation of NADPH at Single-Walled Carbon Nanotubes Functionalized with Poly(Nile Blue A). *J. Electroanal. Chem.* **2008**, *624*, 21−26.
(46) Yokota, A.; Sasajima, K.; Yoneda, M. Reactivation of Inactivated D-glucose Dehydrogenase of A Bacillus Species by Pyridine And Adenine Nucleotides. *Agric. Biol. Chem.* **1979**, *43*, 271−278.
(47) Nagao, T.; Mitamura, T.; Wang, X. H.; Negoro, S.; Yomo, T.; Urabe, I.; Okada, H. Cloning, Nucleotide Sequences, and Enzymatic Properties of Glucose Dehydrogenase Isoenzymes from Bacillus Megaterium IAM1030. *J. Bacteriol.* **1992**, *174*, 5013−5020.
(48) Anicet, N.; Anne, A.; Moiroux, J.; Savéant, J.-M. Electron Transfer in Organized Assemblies of Biomolecules. Construction and Dynamics of Avidin/Biotin Co-immobilized Glucose Oxidase/Ferrocene Monolayer Carbon Electrodes. *J. Am. Chem. Soc.* **1998**, *120*, 7115−7116.
(49) Bourdillon, C.; Demaille, C.; Gueris, J.; Moiroux, J.; Savéant, J.-M. A Fully Active Monolayer Enzyme Electrode Derivatized by Antigen-Antibody Attachment. *J. Am. Chem. Soc.* **1993**, *115*, 12264−12269.
(50) Wan, D.; Shaojun, Y.; Li, G. L.; Neoh, K. G.; Kang, E. T. Glucose Biosensor from Covalent Immobilization of Chitosan-Coupled Carbon Nanotubes on Polyaniline-Modified Gold Electrode. *ACS Appl. Mater. Interfaces* **2010**, *2*, 3083−3091.
(51) Si, P.; Ding, S.; Yuan, J.; Lou, X. W.; Kim, D.-H. Hierarchically Structured One-Dimensional TiO_2 for Protein Immobilization, Direct Electrochemistry, and Mediator-Free Glucose Sensing. *ACS Nano* **2011**, *5*, 7617−7626.

DOI: 10.1021/am506758u
ACS Appl. Mater. Interfaces 2015, 7, 584−592